Engineered Mutants of a Marine Photosynthetic Purple Nonsulfur Bacterium with Increased Volumetric Productivity of Polyhydroxyalkanoate Bioplastics

AUTHOR(S):

Foong, Choon Pin; Higuchi-Takeuchi, Mieko; Ohtawa, Kenji; Asai, Takuya; Liu, Hanqin; Ozeki, Yasuyuki; Numata, Keiji

CITATION:

Foong, Choon Pin ...[et al]. Engineered Mutants of a Marine Photosynthetic Purple Nonsulfur Bacterium with Increased Volumetric Productivity of Polyhydroxyalkanoate Bioplastics. ACS Synthetic Biology 2022, 11(2): 909-920

ISSUE DATE:

2022-02-18

URL:

http://hdl.handle.net/2433/282829

ACS Synthetic Biology

pubs.acs.org/synthbio Research Article

Engineered Mutants of a Marine Photosynthetic Purple Nonsulfur Bacterium with Increased Volumetric Productivity of Polyhydroxyalkanoate Bioplastics

Choon Pin Foong, Mieko Higuchi-Takeuchi, Kenji Ohtawa, Takuya Asai, Hanqin Liu, Yasuyuki Ozeki, and Keiji Numata*

Cite This: *ACS Synth. Biol.* 2022, 11, 909–920 Read Online

ACCESS | Metrics & More | Article Recommendations | Supporting Information

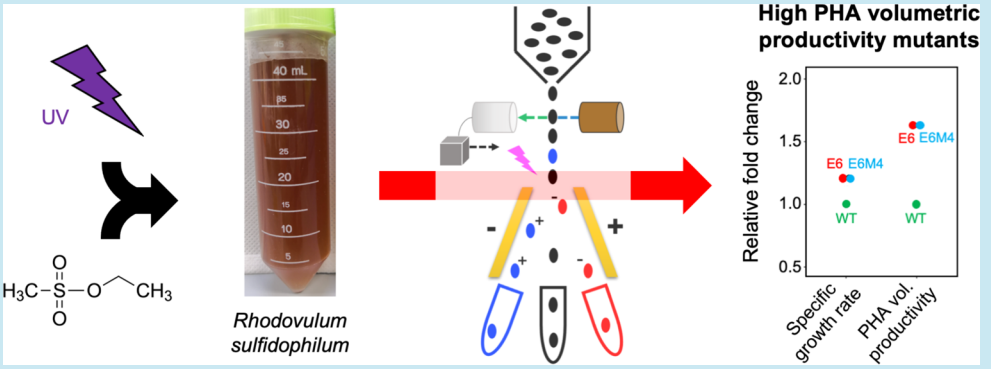

ABSTRACT: Polyhydroxyalkanoates (PHAs) are green and sustainable bioplastics that could replace petrochemical synthetic plastics without posing environmental threats to living organisms. In addition, sustainable PHA production could be achieved using marine photosynthetic purple nonsulfur bacteria (PNSBs) that utilize natural seawater, sunlight, carbon dioxide gas, and nitrogen gas for growth. However, PHA production using marine photosynthetic PNSBs has not been economically feasible yet due to its high cost and low productivity. In this work, strain improvement, using genome-wide mutagenesis coupled with high-throughput screening via fluorescence-activated cell sorting, we were able to create *Rhodovulum sulfidophilum* mutants with enhanced volumetric PHA productivity, with an up to 1.7-fold increase. The best selected mutants (E6 and E6M4) reached the stationary growth phase 1 day faster and accumulated the maximum PHA content 2 days faster than the wild type. Maximizing volumetric PHA productivity before the stationary growth phase is indeed an additional advantage for *R. sulfidophilum* as a growth-associated PHA producer.

KEYWORDS: *strain improvement, genome-wide mutagenesis, fluorescence-activated cell sorting, Rhodovulum sulfidophilum, microbial cell factory, biopolymer*

Synthetic fossil-based plastics have been widely integrated into the contemporary human lifestyle due to their low cost, low weight, easy accessibility, and high durability. Indeed, these long-lasting and nonbiodegradable synthetic polymers have accumulated in landfills or natural environments (~80%) since their invention over 100 years ago due to difficulties in the recycling process (<10%) and negligence in disposal.[1] In addition, the production and incineration of synthetic plastics also leads to the emission of greenhouse gases (GHGs) (~3.5% of global annual GHG emissions).[2] Moreover, partially degraded synthetic plastics released xenobiotic contaminants such as microplastics and volatile organic compounds, which have been recently discovered to be unseen hazards to living organisms.[3,4]

Alternative solutions for synthetic plastics would ideally fit two key criteria: (i) the material itself must be completely biobased, biodegradable, and biocompatible, and (ii) the bioprocess and end-of-life of the bioplastics must be green and sustainable. Since the 1980s, industrial production of bioplastics such as polyhydroxyalkanoates (PHAs), polylactic acid, and polybutylene succinate (PBS) has been initiated due to the crude oil and energy crises. Global production of PHAs is expected to increase 10-fold by 2025 from ~36,000 tons in 2020.[5] PHAs are naturally synthesized by many prokaryotes and demonstrate physicochemical and mechanical properties similar to those of fossil-based synthetic plastics. PHAs are

Received: October 25, 2021
Published: January 21, 2022

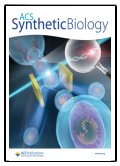

https://doi.org/10.1021/acssynbio.1c00537
ACS Synth. Biol. 2022, 11, 909–920

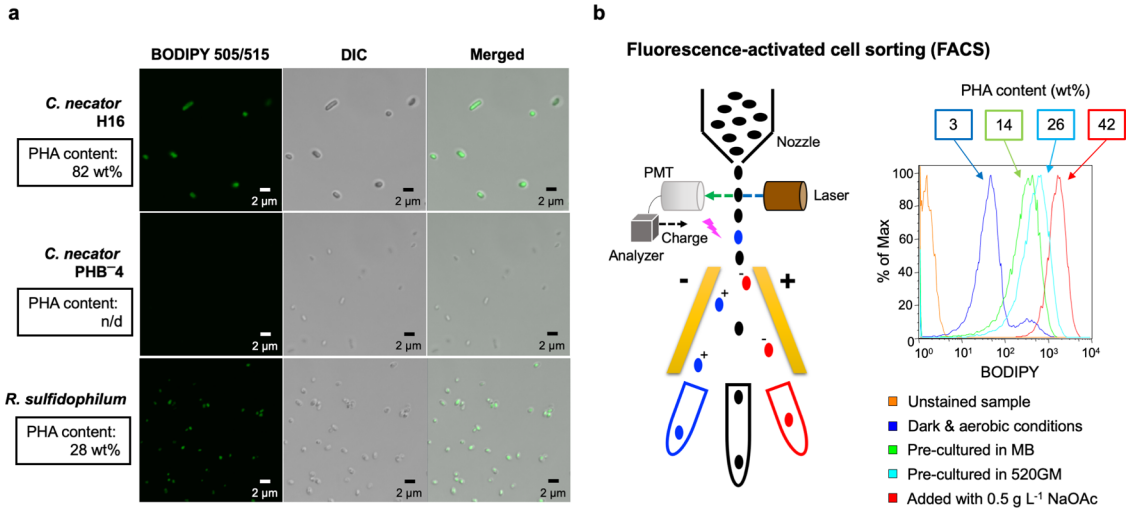

Figure 1. Fluorescence microscopy imaging and flow cytometry analysis of PHA accumulation in bacteria. (a) The presence of PHA in *C. necator* H16 and *R. sulfidophilum* was detected by BODIPY 505/515 fluorescence staining (Ex./Em.: 488/510), while no fluorescence or PHA was detected in *C. necator* PHB⁻4. Scale bars = 2 μm. (b) *R. sulfidophilum* cells from various culture conditions were collected, stained with BODIPY 505/515, and analyzed by flow cytometry. The samples showed different fluorescence intensities (*X*-axis, BODIPY) depending on the PHA content. The target cells could be sorted out selectively in tiny liquid droplets labeled with electric charges.

biodegradable under both aerobic and anaerobic conditions[6] and in various environments, such as soil, freshwater, and seawater.[7] The biocompatibility features of PHAs have been tested in various biomedical applications, as reviewed by Koller (2018)[8] and Luo et al. (2019).[9]

Heterotrophic bacteria such as wild-type or recombinant *Cupriavidus* spp. and *Pseudomonas* spp. have long been established as mainstream PHA producers.[10] In recent years, cyanobacteria and purple bacteria possessing photosynthetic and nitrogen fixation abilities have been explored as next-generation PHA producers to promote sustainable bioprocesses, prevent competition for organic carbon and nitrogen sources in food- and agriculture-based sectors, and reduce GHG levels in the atmosphere.[11,12] In addition, PHA production using halophiles has also been investigated to reduce freshwater consumption and lower contamination risks.[13,14] The marine photosynthetic purple nonsulfur bacterium (PNSB) *Rhodovulum sulfidophilum* is a weak halophile and is able to produce PHAs in a growth-associated manner.[15,16] *R. sulfidophilum* has been proposed as an ideal and sustainable platform for the production of high-value compounds such as biohydrogen, PHAs, and spider silk.[12,17,18]

However, the productivity of PHAs in *R. sulfidophilum* is relatively low (~20 to 30 wt % of cell dry mass) due to the low substrate affinity of PHA synthase ($PhaC_{Rs}$),[19] and this species is economically uncompetitive compared to the current heterotrophic workhorses. Therefore, in this work, our aim was to enhance the PHA volumetric productivity of *R. sulfidophilum* using a synthetic biology approach, focusing on faster cell growth and higher PHA accumulation. Generally, this could be achieved by genome-wide mutagenesis, adaptive laboratory evolution, or targeted metabolic engineering.[20−24] Genome-wide mutagenesis is preferable due to the highly complex cellular metabolic processes in metabolically versatile photosynthetic PNSBs, which are affected by light, oxygen, and carbon source availability.[25,26] In addition, rapid and high-throughput single-cell mutant screening of high PHA-accumulating *R. sulfidophilum* via fluorescence-activated cell sorting (FACS), which has not been reported previously in PHA studies, is introduced in this work.

RESULTS AND DISCUSSION

Evaluation of Mutagenesis Conditions for *Rhodovulum sulfidophilum*. Mutagenesis conditions were optimized by introducing ethyl methanesulfonate (EMS) at various concentrations (0.25, 0.50, 0.75, and 1.00% v/v), varying the EMS incubation period (20, 40, and 60 min), and applying various ultraviolet (UV) irradiation dosages (10, 20, 30, 50, and 100 J m^{-2}) to the *R. sulfidophilum* cultures. As expected, the survival rate of *R. sulfidophilum* decreased under harsher conditions, such as higher EMS concentrations, longer EMS incubation periods, or higher UV irradiation dosages (Figure S1). Eventually, *R. sulfidophilum* cultures under mutagenesis conditions that exhibited 10−60% survival rates (Table S1) were chosen for subsequent PHA induction and flow cytometry analysis for identification of high PHA-accumulating mutants.

Flow Cytometry-Based High-Throughput Screening of High PHA-Accumulating *R. sulfidophilum* Mutants. First, the specificity of BODIPY 505/515 staining on intracellular PHAs was examined by using confocal laser scanning fluorescence microscopy. Both wild-type *Cupriavidus necator* H16 and wild-type *R. sulfidophilum* showed positive intracellular fluorescence emissions under PHA-accumulating conditions. On the other hand, no fluorescence emission was observed inside the cells of *C. necator* PHB⁻4, which is a PHA-negative mutant (Figure 1a). Next, the sensitivity of BODIPY 505/515 staining in flow cytometry analysis was evaluated by using wild-type *R. sulfidophilum* with varying PHA levels [3−42 wt %, confirmed by gas chromatography−mass spectrometry (GC−MS) analysis] under different cultivation conditions (Table S2; Figure 1b).

BODIPY 493/503 has been used for rapid PHA quantification in yeast and bacteria by flow cytometry,[27−29] while BODIPY 505/515 has been used to detect intracellular PHA granules by fluorescence microscopy.[30] In this study, BODIPY 505/515 was used for PHA detection in flow

https://doi.org/10.1021/acssynbio.1c00537
ACS Synth. Biol. 2022, 11, 909−920

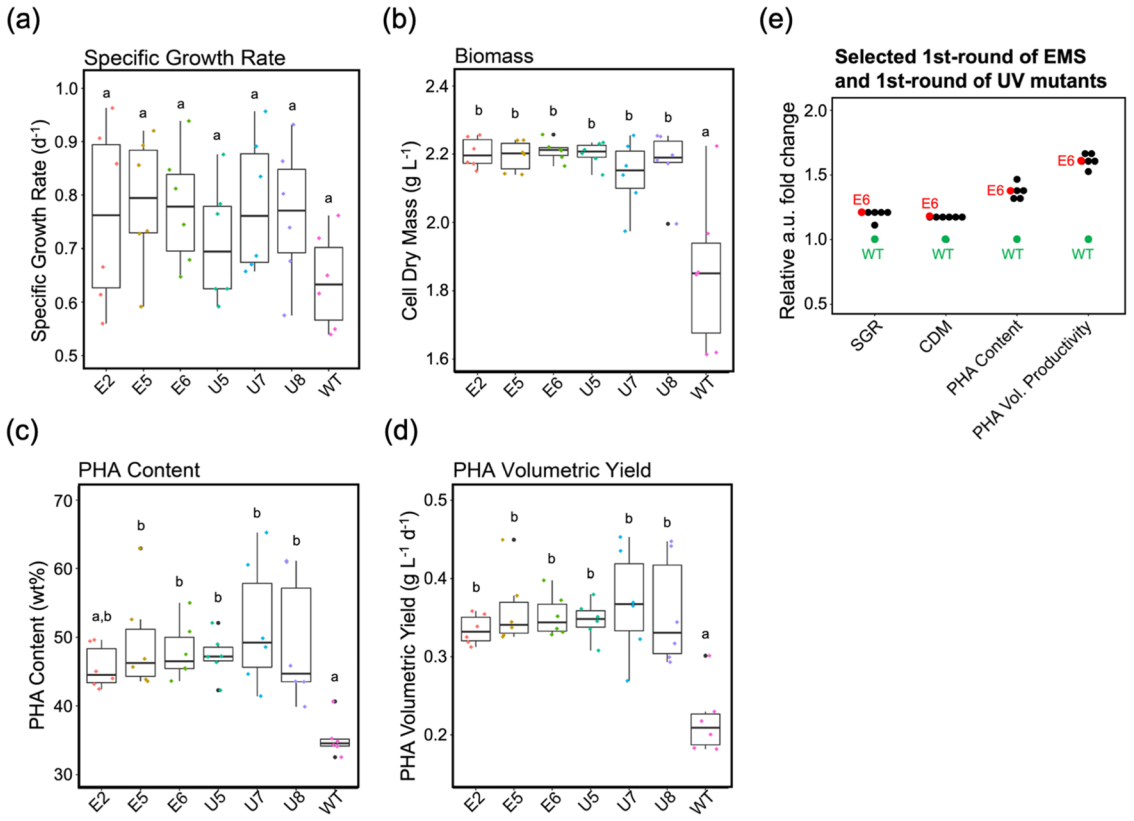

Figure 2. Scale-up confirmation of fast growing and high PHA-accumulating *R. sulfidophilum* mutants from the 1st round of EMS treatment and the 1st round of UV treatment. (a) Specific growth rate, (b) cell dry mass, (c) PHA content, (d) volumetric PHA productivity, and (e) relative fold changes compared to the wild type. Boxplot data accompanied by different superscripted letters are significantly different (Tukey's HSD, $p < 0.05$, $n = 6$, two independent experiments). Cells were harvested from 3-day 50-mL cultures grown in 520GM at 30 °C under LED 730 nm and 30 Wm^{-2} irradiation.

cytometry analysis and for FACS of PHA-accumulating bacterial cells.

Mutants Generated from the 1st Round of Mutagenesis Treatments. In the 1st round of mutagenesis treatments, 14 mutagenized samples with 10−60% survival rates (11 EMS-treated and 3 UV-treated, Table S1) were subjected to flow cytometry analysis (Figure S2a). High PHA-accumulating *R. sulfidophilum* mutants were sorted out with the gating criterion set as ∼0.1% of the total cell population with the highest fluorescence signal. Single colonies of FACS-sorted high PHA-accumulating mutants were further screened for rapid growth under microscale culture conditions by assessing the specific growth rate (SGR) based on optical density (OD) (Figure S3a,b). A total of 35 single colonies of mutants were screened in the 1st round of EMS treatment, and 71% of them exhibited a higher SGR (≥1.1-fold) than the wild-type strain. In the 1st round of UV treatment, a total of nine single colonies of mutants were screened, and 78% of them exhibited a higher SGR (≥1.1-fold) than the wild-type strain.

After an initial scale-up evaluation, only the top three mutants with the highest volumetric PHA productivity from the 1st-round EMS treatment (E2, E5, and E6) and the 1st-round UV treatment (U5, U7, and U8) were chosen for the final phenotype assessment (Figure S4a,b). No significant differences were observed in the SGR. All six mutants exhibited a significantly higher cell biomass (1.2-fold increase), PHA content (1.3- to 1.5-fold increase), and volumetric PHA productivity (1.5- to 1.7-fold increase) than the wild-type strain (Figure 2). However, no significant differences were observed among the selected mutants except for E2, which showed a slightly lower PHA content (Figure 2c). Eventually, E6 was chosen and taken forward to the 2nd round of mutagenesis treatment.

Mutants Generated from the 2nd Round of Mutagenesis Treatments. In the 2nd round of mutagenesis treatments, three mutagenized samples with 27−49% survival rates (one EMS-treated and two UV-treated, Table S1) were subjected to flow cytometry analysis (Figure S2b) and FACS with the same gating criterion setting as mentioned previously. A total of nine E6-derived single colonies of mutants were screened under microscale culture conditions, but only the E6V1 mutant showed a higher SGR (≥1.1-fold) than the wild type (Figure S3c).

After an initial scale-up evaluation, only E6V1 and E6M4 showed improved volumetric PHA productivity compared to their parental E6 mutant and were subjected to the final phenotype assessment (Figure S4c). No significant differences were observed in the SGR. E6V1 and E6M4 exhibited a significantly higher cell biomass (1.2-fold increment), PHA content (1.4-fold increment), and volumetric PHA productivity (1.6- to 1.7-fold increment) than the wild type but showed no significant difference compared to the parental E6 (Figure 3). Thus, no further phenotypic improvements were observed in cell growth and volumetric PHA productivity after E6 was subjected to an additional round of mutagenesis treatment.

Moreover, intracellular PHA accumulation in *R. sulfidophilum* was also examined by stimulated Raman scattering (SRS) microscopy, which is a label-free technique based on molecular

https://doi.org/10.1021/acssynbio.1c00537
ACS Synth. Biol. 2022, 11, 909−920

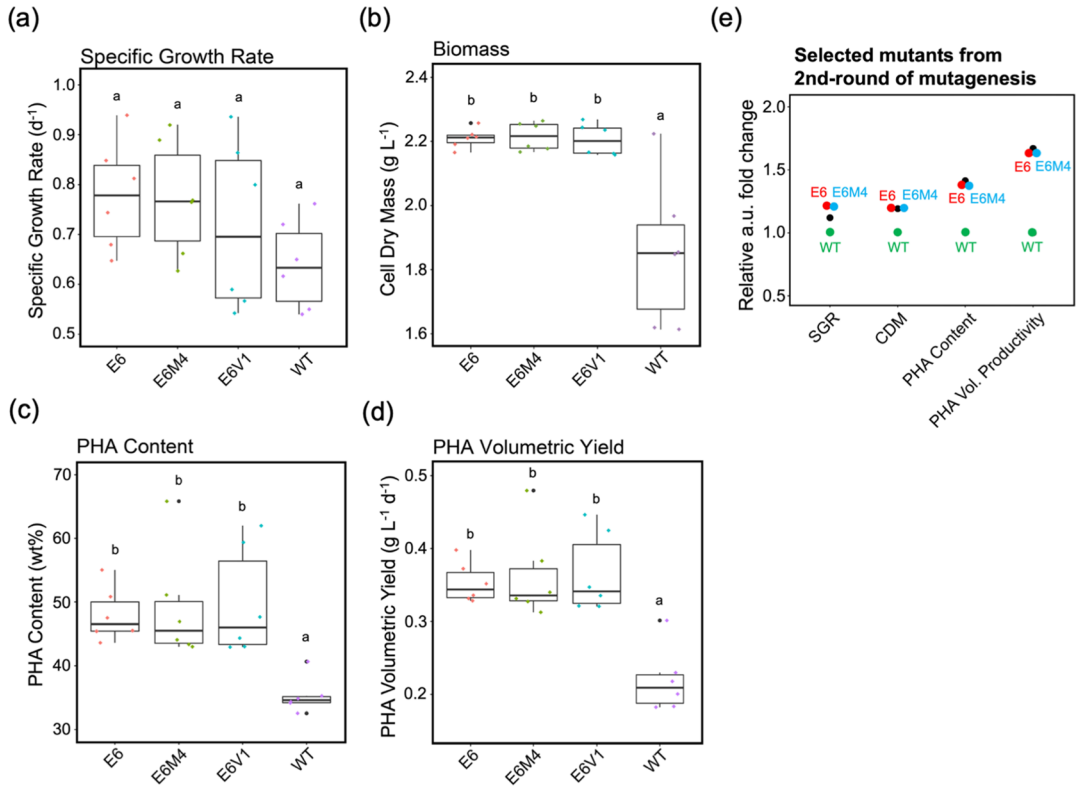

Figure 3. Scale-up confirmation of fast growing and high PHA-accumulating *R. sulfidophilum* mutants from the 2nd round of mutagenesis. (a) Specific growth rate, (b) cell dry mass, (c) PHA content, (d) volumetric PHA productivity, and (e) relative fold changes compared to the wild type. Boxplot data accompanied by different superscripted letters are significantly different (Tukey's HSD, $p < 0.05$, $n = 6$, two independent experiments). Cells were harvested from 3-day 50-mL cultures grown in 520GM at 30 °C under LED 730 nm and 30 Wm^{-2} irradiation.

vibration. SRS microscopy was also able to distinguish low PHA-accumulating cells (WT_L) from medium to high PHA-accumulating cells (WT_H, WT_M, and mutants) (Figure S5). This technique could be coupled with flow cytometry and image-activated cell sorting for high-throughput analysis and screening of heterogeneous samples.[31,32]

Time Course Profiles of Cell Growth and PHA Accumulation for the Wild Type and the E6 and E6M4 Mutants. In brief, E6 and E6M4 did not show significant differences in maximum cell biomass, but significant differences were observed in the maximum PHA content and maximum volumetric PHA productivity compared to the wild type (Figure 4). Overall, E6 and E6M4 grew relatively fast after 5 h and reached the stationary growth phase ($OD_{660} \sim 5$; CDM ~2.6 gL^{-1}) 1 day earlier than the wild-type strain (Figure 4a,b). In addition, E6 and E6M4 also exhibited relatively fast PHA accumulation after 41 h and reached the maximum PHA content 2 days earlier than the wild-type strain (Figure 4c,d). At 53 h, both the mutants and wild type had reached the highest volumetric PHA productivity, but the productivity of the mutants was significantly (1.6-fold) better than that of the wild type (16 ± 1 vs 10 ± 3 mgL^{-1} h^{-1}).

Genomic Analysis of *R. sulfidophilum* Mutants with High Volumetric PHA Productivity. Whole-genome sequencing was performed for wild-type *R. sulfidophilum* and the E6 and E6M4 mutants to identify possible mutations that enhanced both cell growth and PHA accumulation. The obtained DNA sequences were mapped to the published genome of *R. sulfidophilum* DSM 1374 (chromosome, accession number NZ_CP015418). More than 95% of the reads were successfully mapped to the reference genome with an average alignment depth of ~1000×. Only homozygous-type mutations with 100% variant read depth were considered for subsequent analysis. A total of seven single-nucleotide variations (SNVs) or point mutations were detected (Table 1 and Figure 5). As expected, all the SNVs were G/C-to-A/T variants. In general, EMS treatment predominantly introduces alkylation mutations (G/C to A/T transition) in the genome.[33,34]

The seven SNVs generated one stop-gained variant (premature stop codon), two synonymous variants (codon substitutions), three missense variants (amino acid changes), and one upstream gene variant (noncoding sequence) in the mutant genomes. For further discussion, the stop-gained variant that was present in only E6 and low-impact synonymous variants was not considered.

Two missense variants of the coding sequence (CDS) have known annotated functions: (i) "G2277594A" at A6W98_RS10765 encodes a CoA-acylating (methyl)-malonate-semialdehyde dehydrogenase, and (ii) "G3469019A" at A6W98_RS16235 encodes an L-lactate dehydrogenase (LDH). Unfortunately, one missense variant of the CDS, "C2644429T", at A6W98_RS12500 encodes a hypothetical protein that has unknown functions. The only noncoding sequence (nCDS) variant is "C2937910T", located between the "-35 box" and "-10 box" of an unknown promoter, as predicted by BPROM,[35] which probably regulates three genes: (a) *dprA*, a DNA-protecting protein, (b) a type I DNA topoisomerase, and (c) an L,D-transpeptidase (Figure 5).

Metabolic Pathway Analysis of the Mutated Enzymes in E6 and E6M4. (Methyl)malonate-semialdehyde dehydrogenase (MMSDH, EC 1.2.1.27) is involved in uracil and valine

https://doi.org/10.1021/acssynbio.1c00537
ACS Synth. Biol. 2022, 11, 909−920

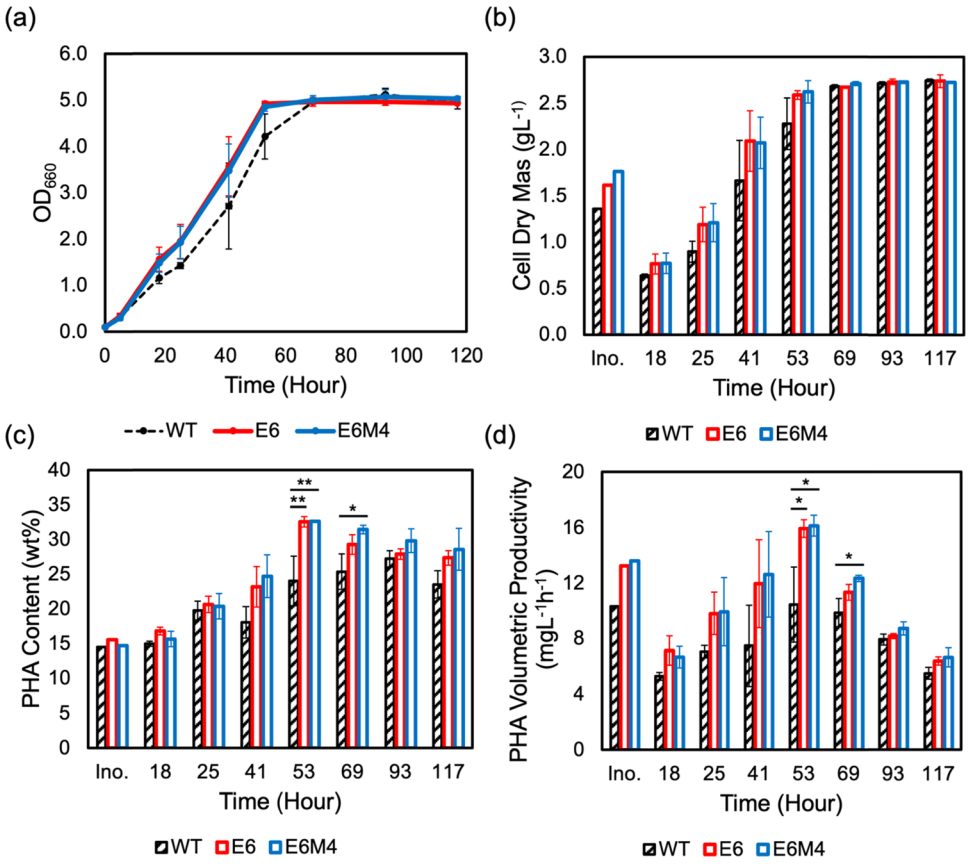

Figure 4. Time course profiles for cell growth and PHA accumulation in *R. sulfidophilum* in a comparison among the wild type and the E6 and E6M4 mutants. (a) OD_{660}, (b) cell dry mass, (c) PHA content, and (d) volumetric PHA productivity. Mean data accompanied by star symbols are significantly different (Tukey's HSD, * $p < 0.05$, ** $p < 0.01$, $n = 3$). Cells were cultured in 15 mL of 520GM at 30 °C under LED 730 nm and 30 Wm^{-2} irradiation. Ino. = inoculum.

Table 1. Single-Nucleotide Variations (SNVs) Detected in E6 and E6M4 Mutants of *R. sulfidophilum* after Filtering with Only Homozygous-Type Mutations and 100% Variant Read Depth: WT = Wild Type; Mt = Mutant

position	sample	WT	Mt	locus tag	type of mutation	annotation
2112710	E6 E6M4	G	A	A6W98_RS10010	synonymous variant	cobaltochelatase subunit CobN
2225781	E6 E6M4	G	A	A6W98_RS10550	synonymous variant	DUF4445 domain-containing protein
2277594	E6 E6M4	G	A	A6W98_RS10765	missense variant	CoA-acylating methylmalonate-semialdehyde dehydrogenase
2644429	E6 E6M4	C	T	A6W98_RS12500	missense variant	hypothetical protein
2937910	E6 E6M4	C	T	non-CDS	upstream gene variant	a. DNA-protecting protein DprA b. Type I DNA topoisomerase c. L,D-transpeptidase
3469019	E6 E6M4	G	A	A6W98_RS16235	missense variant	L-lactate dehydrogenase
4036207	E6	G	A	A6W98_RS18655	stop-gained	crotonyl-CoA carboxylase/reductase

metabolism, which affects acetyl-CoA and propionyl-CoA availability, respectively (Figure 6). The valine catabolism pathway is incomplete in *R. sulfidophilum*; therefore, the effect of propionyl-CoA could be ruled out. In addition, it is difficult to characterize the mutation effect of (methyl)malonate-semialdehyde dehydrogenase biochemically due to the unavailability of commercial enzymatic assays. LDH (EC 1.1.1.27) is involved in carbohydrate metabolism, which affects acetyl-CoA availability. Acetyl-CoA is an important central metabolite intermediate that can be oxidized for energy production via the tricarboxylic acid cycle (TCA cycle) and reduced to PHAs via the "PhaABC" PHA biosynthesis pathway.[36,37] LDH catalyzes the interconversion of pyruvate and lactate at the same rate under the unaltered reaction equilibrium state.[38,39] Nonetheless, there were no significant differences in LDH activity between the mutants and wild type (Figure 7).

Since the mutations were highly likely to affect the acetyl-CoA supply, an in vivo study of acetyl-CoA synthesis from carbon precursors was performed. Four different carbon

https://doi.org/10.1021/acssynbio.1c00537
ACS Synth. Biol. 2022, 11, 909−920

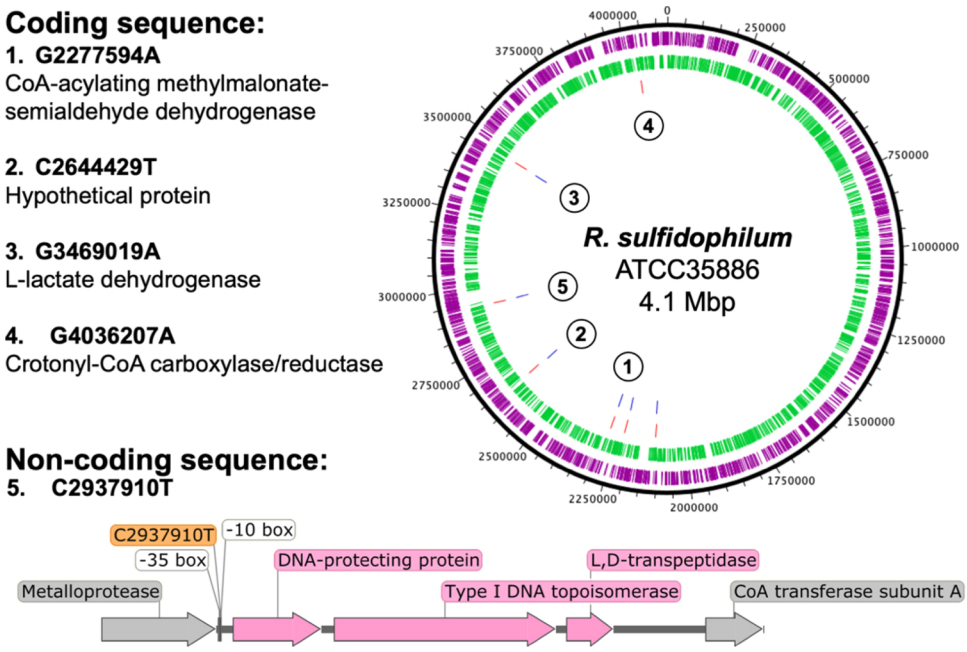

Figure 5. Genomic analysis of wild-type *R. sulfidophilum* and the E6 and E6M4 mutants. The positions of the homozygous SNV (Table 1) are depicted in the genome map. The purple circle represents the CDS in the forward strand, while the green circle represents the CDS in the reverse strand. Red lines are mutations in E6, while blue lines are mutations in E6M4. One stop-gained variant, three missense variants of the CDS, and one upstream gene variant (noncoding sequence) are highlighted and numbered from 1 to 5. Adjacent regions (pink color) of the upstream gene variant that were possibly affected by the mutation are depicted in the lower section.

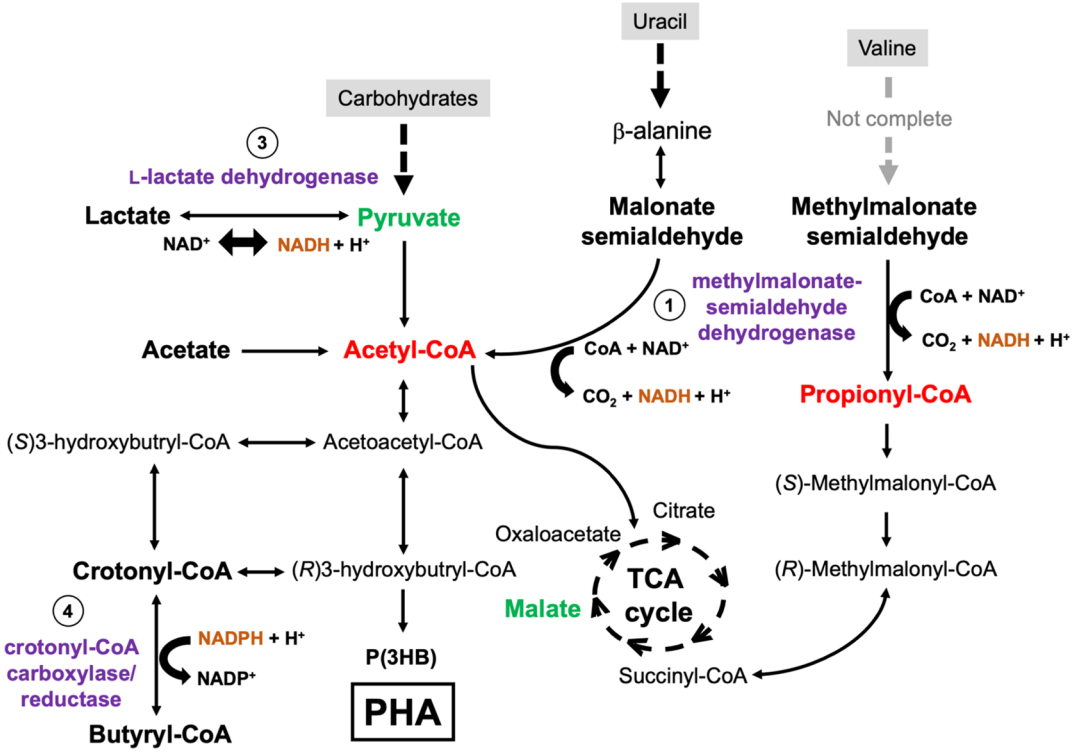

Figure 6. Metabolic pathway analysis of the mutated enzymes in the *R. sulfidophilum* E6 and E6M4 mutants. Enzymes with identified mutations are numbered and colored in purple. 520GM containing sodium pyruvate and sodium L-malate as the main carbon sources (green colored) was used as the selection medium for mutagenized *R. sulfidophilum*.

sources, namely, malate, pyruvate, lactate, and acetate, were examined independently to investigate the carbon assimilation behavior between the mutants and wild type regarding the interconnections of the acetyl-CoA pool and TCA cycle. As a result, mutants supplemented with pyruvate or malate showed significantly faster cell growth in the logarithmic growth phase (~14 to 47 h) and reached the stationary growth phase faster than the wild type (Figure 8a,c). On the other hand, no

https://doi.org/10.1021/acssynbio.1c00537
ACS Synth. Biol. 2022, 11, 909−920

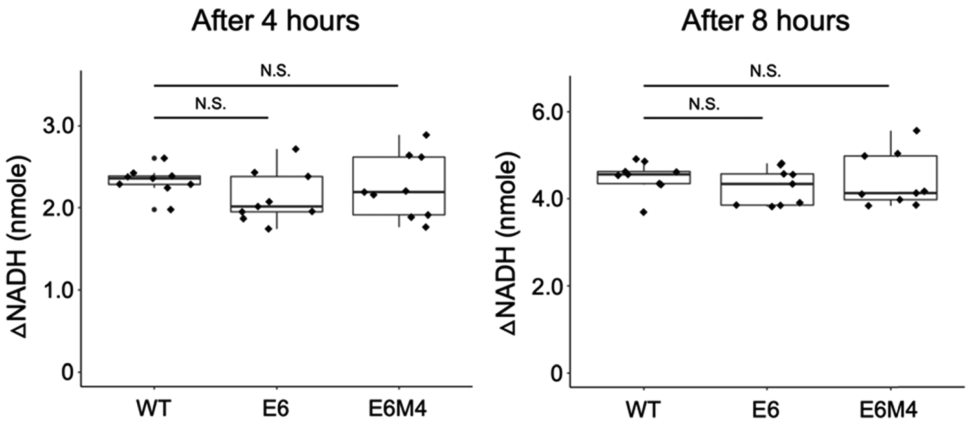

Figure 7. LDH enzymatic activity assay. Changes in NADH levels were quantified after incubation for 4 and 8 h at 30 °C using crude cell lysates from the mutants (E6 and E6M4) and wild type. No significant differences were observed (Tukey's HSD, $p < 0.05$, $n = 9$). N.S. = nonsignificant.

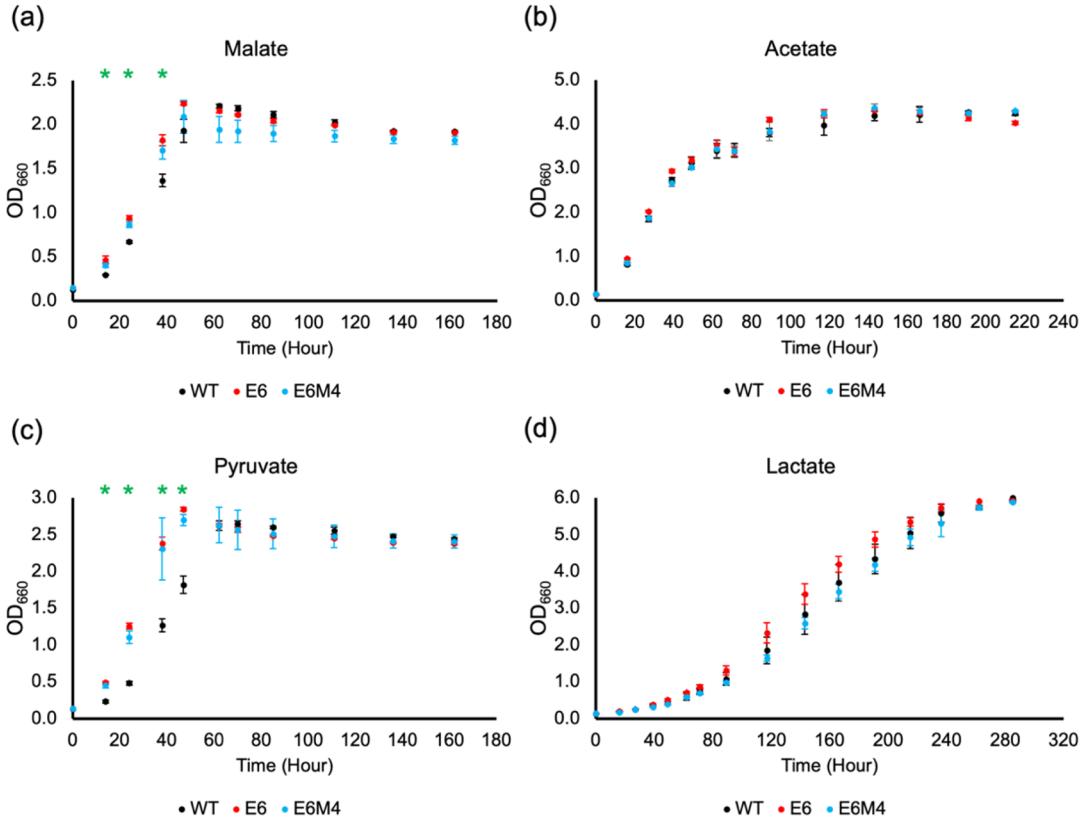

Figure 8. Comparison of cell growth between the mutants (E6 and E6M4) and wild-type *R. sulfidophilum* based on carbon assimilation profiles. (a) Malate, (b) acetate, (c) pyruvate, or (d) lactate was independently used as the main carbon source in 520GM. Mean data accompanied by green star symbols indicate significant differences (Tukey's HSD, $p < 0.01$, $n = 3$) between the mutants and wild type. Cells were cultured in 20 mL 520GM at 30 °C under LED 730 nm and 30 Wm^{-2} irradiation.

significant differences in cell growth were observed when acetate or lactate was provided (Figure 8b,d). In addition, the growth-enhancing effect was stronger for pyruvate than for malate. These results suggested that pyruvate was actively converted to malate (entering the TCA cycle) via malic enzymes and then further converted to oxaloacetate via malate dehydrogenase in the mutants (Figure 9). This is because excessive oxaloacetate and NADH inhibit malate dehydrogenase, which prevents the conversion of malate to oxaloacetate.[40] As shown by a recent study, the same strain of *R. sulfidophilum* has been evaluated for PHA production using different organic acids (acetate, lactate, malate, and succinate) as the sole carbon source.[41] Malate could promote fast cell growth but was the least preferable carbon source for PHA production, at least threefold lower as compared to acetate and lactate. This indicated that malate was mainly used for cell growth instead of being converted to pyruvate or acetyl-CoA for PHA synthesis. In addition, reducing equivalents are present at excessive levels when organic substrates are consumed as carbon and electron sources during photoheterotrophic growth. As reported in a previous study, Calvin−Benson−Bassham cycle mutants in certain PNSBs were incapable of using CO_2 fixation as an electron sink and exhibited growth inhibition due to electron imbalance.[42] In contrast, no excess

https://doi.org/10.1021/acssynbio.1c00537
ACS Synth. Biol. 2022, 11, 909−920

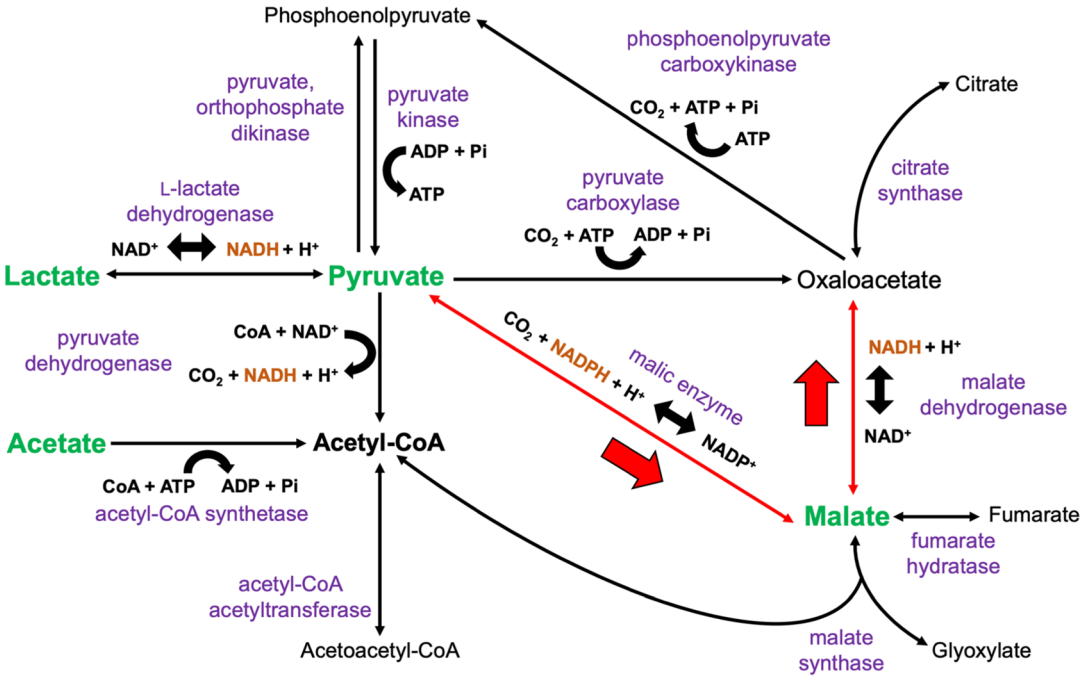

Figure 9. Carbon assimilation pathways for malate, acetate, pyruvate, and lactate in *R. sulfidophilum*. The possible enzymatic reactions that were favorable in the E6 and E6M4 mutants are highlighted with red-colored arrows. The enhanced rapid growth phenotype in the mutants was probably due to a better redox regulation ability, which allowed the strain to rapidly utilize excessive reducing equivalents [NAD(P)H] when using pyruvate and/or malate as the main carbon sources.

reducing equivalents were produced when acetate was used as the main carbon source.

It is also interesting to note that the differences in growth occurred only at the logarithmic growth phase, while the maximum OD_{660} at the stationary growth phase was almost the same between the mutant and wild type when malate or pyruvate was added (Figure 8a,c). This suggested that the mutants could respond to the change more rapidly by balancing the cellular redox levels. Thus, a better oxidation−reduction (redox) status regulation ability could be the main reason for the rapid growth phenotype in the presence of malate and/or pyruvate. One possible factor regulating the redox status is the presence of three oligomeric forms (dimer, tetramer, and octamer) of malate dehydrogenase in *Rhodovulum* species; these forms are involved in rapid equilibration of the NADH/NAD^+ and malate/oxaloacetate ratios according to cultivation conditions.[43] However, it is unclear at this point how redox regulation works differently in the mutants, which still requires further investigation.

CONCLUSIONS

A synthetic biology-based strain improvement approach using genome-wide mutagenesis and high-throughput FACS greatly simplified the desired mutant generation and screening processes, especially for microorganisms possessing highly complex cellular metabolism. This approach enabled us to generate *R. sulfidophilum* mutants that exhibited up to 1.7-fold higher volumetric PHA productivity and accumulated the maximum PHA content 2 days faster than the wild type. These improved phenotypes conferred advantages to *R. sulfidophilum* as a promising sustainable PHA production platform by reducing PHA production costs.

METHODS

Media Compositions and Culture Conditions. *R. sulfidophilum* DSM1374/ATCC35886/W4,[44,45] a marine photosynthetic PNSB, was obtained from the American Type Culture Collection (ATCC). For culture maintenance purposes, *R. sulfidophilum* was grown on marine agar or in marine broth (BD Difco, USA) at 30 °C with continuous exposure to far-red LED light (730 nm, 30 Wm^{-2}). For the purpose of PHA biosynthesis, *R. sulfidophilum* was grown in 520-Growth Medium (520GM), which contained the following components per liter: 0.5 g of KH_2PO_4, 0.25 g of $CaCl_2 \cdot 2H_2O$, 3.0 g of $MgSO_4 \cdot 7H_2O$, 0.68 g of NH_4Cl, 20 g of NaCl, 3.0 g of sodium L-malate, 3.0 g of sodium pyruvate, 0.4 g of yeast extract, 2 mg of vitamin B12, 0.25 mg of ferric citrate and micronutrients, including 70 μg of $ZnCl_2$, 100 μg of $MnCl_2 \cdot 4H_2O$, 60 μg of H_3BO_3, 200 μg of $CoCl_2 \cdot 6H_2O$, 20 μg of $CuCl_2 \cdot 2H_2O$, 20 μg of $NiCl_2 \cdot 6H_2O$, and 40 μg of $Na_2MoO_4 \cdot 2H_2O$. The pH of the medium was adjusted to 7.0 before autoclave sterilization.[16]

Growth Profile and Cell Biomass Analyses. The growth profile of *R. sulfidophilum* was determined based on the OD, measured using a UV/vis spectrophotometer as the absorbance at 660 nm. Specific growth rates (μ values) were calculated based on the slope of the growth curve.[46] Total cell biomass was determined based on the cell dry mass of the samples after lyophilization.

PHA Biosynthesis. PHA biosynthesis experiments were conducted via one-stage batch cultivation in 50 mL of 520GM in a 50-mL conical centrifuge tube. *R. sulfidophilum* was first precultured in 15 mL of 520GM until the OD_{660} reached ∼2.0 (logarithmic phase) before being transferred to fresh 520GM at an initial cell density (OD_{660}) of ∼0.15. *R. sulfidophilum* cultures were incubated at 30 °C with continuous exposure to far-red LED light (730 nm, 30 Wm^{-2}) for 3−5 days or before

https://doi.org/10.1021/acssynbio.1c00537
ACS Synth. Biol. 2022, 11, 909−920

the cultures reached the stationary phase. The bacterial cells were harvested by centrifugation at 9000 ×*g* for 10 min, washed once with distilled water, kept at −80 °C overnight, and finally lyophilized for 24 h.

PHA Quantification. The PHA content and composition were determined by GC−MS analysis.[16] Approximately 2 mg of lyophilized cells was subjected to methanolysis [1 mL of chloroform and 1 mL of methanolysis solution (methanol/sulfuric acid, 85:15 v/v)] at 100 °C for 140 min. After cooling to room temperature, 1 mL of phosphate buffer (pH 8) was added to the reaction mixture, which was then vortex-mixed and neutralized with 0.5 N NaOH. The lower chloroform layer was transferred to a glass tube containing anhydrous sodium sulfate to remove the water content. The samples were analyzed with a GCMS-QP2010 Ultra GC−MS instrument (Shimadzu, Japan) equipped with a 30 m × 0.25 mm DB-1 capillary gas chromatography column (Agilent Technologies, USA). For analysis, 1 μL of sample was injected with helium as a carrier gas (3.30 mL min^{-1}). The following temperature program was used to separate ethyl esters: 45 °C for 1 min, temperature ramp of 7 °C per min to 117 °C. The interface and ion source temperatures were 250 and 230 °C, respectively.

Generation of *R. sulfidophilum* Mutants. Genome-wide mutagenesis was performed on *R. sulfidophilum* using two different approaches: (i) chemical mutagenesis by using EMS and (ii) physical mutagenesis by using UV irradiation. In both approaches, mid-logarithmic-phase cultures of *R. sulfidophilum* in marine broth (OD_{660} ∼ 1.2) were prepared, and 1 mL of the culture was centrifuged at 10,000 ×*g* for 3 min. For EMS mutagenesis,[34] the cell pellet was washed twice in cold 1 × A buffer [60 mM K_2PO_4, 33 mM KH_2PO_4, 7.6 mM $(NH_4)_2SO_4$, and 1.7 mM sodium citrate; pH 7] and resuspended in cold 2 × A buffer. EMS was added to the samples (i) at final concentrations of 0, 0.25, 0.50, 0.75, and 1.00% and (ii) with incubation periods of 0, 10, 20, 30, and 60 min at 30 °C and 180 rpm under dark conditions. After EMS treatment, the samples were immediately centrifuged at 10,000 ×*g* for 3 min, washed twice with cold 1 × A buffer, resuspended in 1 mL of marine broth and finally spread-plated on marine agar with different dilution factors. The plates were incubated at 30 °C with continuous exposure to far-red LED light (730 nm, 30 Wm^{-2}) until colonies appeared (∼3 to 4 days).

For UV mutagenesis,[47] the cell pellet was washed twice in cold 0.1 M sodium phosphate (pH 7.0) and resuspended in cold 0.1 M sodium phosphate (pH 7.0). A total of 1 mL of sample was loaded into each well of a 6-well flat-bottom plate. The samples were exposed to UV irradiation (wavelength ∼ 254 nm) using a CX-2000 Ultraviolet Crosslinker (Analytik Jena, USA) at dosages of 0, 25, 50, 100, 150, and 200 Jm^{-2}. All the samples were immediately recovered from the 6-well flat-bottom plate and finally spread-plated on marine agar with different dilution factors. The plates were incubated in a container covered with an Asmetec SFG10 filter to prevent photolyase reactivation (by removing light with wavelengths <520 nm) at 30 °C with continuous exposure to far-red LED light (730 nm, 30 Wm^{-2}) until colonies appeared (∼3 to 4 days). The number of colonies formed on the marine agar plates was recorded, and survival rates were calculated based on the number of colony forming units (cfu).

Fluorescence Microscopy Imaging. Cells at the late logarithmic growth phase in 520GM culture were collected by centrifugation at 10,000 ×*g* for 3 min. The supernatant was discarded, and the cells were resuspended in 1 × PBS containing 5 μM BODIPY 505/515 (4,4-difluoro-1,3,5,7-tetramethyl-4-bora-3a,4a-diaza-s-indacene) (Thermo Fisher Scientific, USA), incubated for 20 min in the dark, and then visualized by confocal laser scanning microscopy (LSM 770) (Zeiss, Germany). The fluorescence was excited with an argon laser (488 nm) and detected at emission wavelengths of 510−520 nm.

Flow Cytometry Analysis and Cell Sorting. One milliliter of late logarithmic growth-phase *R. sulfidophilum* culture in 520GM was harvested by centrifugation at 10,000 ×*g* for 3 min. The cell pellet was resuspended in 1 mL of 520GM and stained with 5 μM BODIPY 505/515 for 20 min in the dark. Both stained and nonstained samples were diluted to ∼1 × 10^6 cells per mL before analysis using a BD FACSAria II Special Order System (BD Biosciences, USA). A blue laser (488 nm) was used to excite BODIPY 505/515. To sort out the desired high PHA-accumulating mutants, the gating criterion was set as ∼0.1% of the total cell population with the highest fluorescence signal. Approximately 10,000−16,000 events were analyzed for each mutagenized sample. A total of five events were sorted into 1 mL of 520GM, incubated for 3 days at 30 °C under continuous exposure to far-red LED light (730 nm, 30 Wm^{-2}), and then spread-plated on marine agar plates (with serial dilutions) to obtain single colonies of mutants.

Microplate-Scale Screening. A single colony of mutated *R. sulfidophilum* from marine agar was inoculated into 200 μL of 520GM in a 96-well microplate. Bacterial cell growth was measured by using a SpectraMax M3 microplate reader (Molecular Devices, USA) to determine the OD_{660}.

SRS Microscopy Imaging. Cells at the late logarithmic growth phase in 520GM culture were collected by centrifugation at 10,000 ×*g* for 3 min, and the cell pellet was resuspended in 520GM. The samples were visualized with an SRS imaging system as previously reported.[48,49] Briefly, pump (790 nm) and Stokes (∼1030 nm) pulses were combined with a dichroic mirror and sent to a laser scanning SRS microscope, where the pulses were focused using a water immersion objective lens on a sample sandwiched by two cover slips. Field of view was 60 × 60 $μm^2$. The Raman signal of intracellular PHA was measured in the wavenumber range of 2800−3100 cm^{-1}. The spectral peak at 2930 cm^{-1} was used for the quantification of PHA in the single cell of interest. The aromatic CH stretching mode of polystyrene beads at 3050 cm^{-1} was used as an internal control for signal normalization.

DNA Extraction, Genome Sequencing, and Analyses. Genomic DNA extraction was carried out for the wild-type *R. sulfidophilum* DSM1374 and mutants E6 and E6M4 using the DNeasy Blood & Tissue Kit (QIAGEN, Germany) according to the manufacturer's protocol. The purified gDNA was quantified using a Nanodrop 1000 (Thermo Fisher Scientific, USA) and stored at −20 °C. Next-generation sequencing (NGS) was outsourced to Macrogen Corp., Japan. Genome sequencing was performed using an Illumina NovaSeq6000 with 151-bp paired-end reads. The NGS library was prepared using an Illumina TruSeq Nano DNA Library Prep Kit. Sequence mapping and variant analysis were conducted with Macrogen's in-house bioinformatics pipeline. In brief, quality filtering of the raw sequence reads was performed using Fastp (v0.19.4), the filtered reads were mapped to the reference genome of *R. sulfidophilum* DSM1374 (GCF_001633165.1) using BWA (v0.7.17), duplicated reads were removed using

https://doi.org/10.1021/acssynbio.1c00537
ACS Synth. Biol. 2022, 11, 909−920

Sambamba (v0.6.7), and, finally, genetic variant annotation and functional effect prediction were performed using SnpEff (v4.3t). A genome map was constructed using DNAPlotter within Artemis software (v18.1.0).[50] Metabolic pathway analysis was performed using the Kyoto Encyclopedia of Genes and Genomes (KEGG) Pathway Database.[51]

Statistical Analysis. Statistical analysis was carried out using R (v3.6.3)[52] with the "ggplot2"[53] and "multcomp" packages.[54] One-way analysis of variance (ANOVA) and Tukey's honest significant difference test were performed for multiple pairwise comparisons between the means of groups.

LDH Activity Assay. The E6 and E6M4 mutants and wild-type *R. sulfidophilum* were cultivated in marine broth until the stationary growth phase. The cells were collected by centrifugation at 10,000 ×*g* for 3 min and resuspended in lysis buffer (50 mM Tris−HCl, 200 mM NaCl, 5% glycerol; pH 7.5). The cell suspensions were kept in an ice-water bath and lysed with a Q125 sonicator (Qsonica, USA) with the amplitude set at 30% and a 2 s ON/10 s OFF cycle for 10 min. The cell lysates were centrifuged at 10,000 ×*g* for 3 min, the supernatant was collected, and the total protein was quantified using the Pierce BCA Protein Assay Kit (Thermo Fisher Scientific, USA). LDH activity was measured using the Lactate Dehydrogenase Activity Assay Kit (Sigma-Aldrich, USA) according to the manufacturer's protocol. LDH catalyzes the interconversion of pyruvate and lactate at the same rate under the unaltered reaction equilibrium state. LDH activity could be determined in either forward or reverse directions. In this kit, LDH reduces NAD to NADH, which was specifically detected by measuring the OD_{450} using a SpectraMax M3 microplate reader (Molecular Devices, USA). The reaction was carried out at 30 °C.

■ ASSOCIATED CONTENT

Supporting Information

The Supporting Information is available free of charge at https://pubs.acs.org/doi/10.1021/acssynbio.1c00537.

> Mutagenesis conditions and survival rate; cultivation conditions for different PHA contents; flow cytometry analysis; microscale screening of fast growing mutants; initial scale-up evaluation of targeted phenotypes; and stimulated Raman scattering (SRS) microscopy analysis (PDF)

■ AUTHOR INFORMATION

Corresponding Author

Keiji Numata − *Department of Material Chemistry, Graduate School of Engineering, Kyoto University, Kyoto 615-8246, Japan; Biomacromolecules Research Team, RIKEN Center for Sustainable Resource Science, Saitama 351-0198, Japan;* orcid.org/0000-0003-2199-7420; Email: numata.keiji.3n@kyoto-u.ac.jp

Authors

Choon Pin Foong − *Department of Material Chemistry, Graduate School of Engineering, Kyoto University, Kyoto 615-8246, Japan*

Mieko Higuchi-Takeuchi − *Biomacromolecules Research Team, RIKEN Center for Sustainable Resource Science, Saitama 351-0198, Japan*

Kenji Ohtawa − *Support Unit for Bio-Material Analysis, Research Resources Division, RIKEN Center for Brain Science, Saitama 351-0198, Japan*

Takuya Asai − *Department of Electrical Engineering and Information Systems, The University of Tokyo, Tokyo 113-8656, Japan*

Hanqin Liu − *Department of Electrical Engineering and Information Systems, The University of Tokyo, Tokyo 113-8656, Japan*

Yasuyuki Ozeki − *Department of Electrical Engineering and Information Systems, The University of Tokyo, Tokyo 113-8656, Japan;* orcid.org/0000-0002-9004-0799

Complete contact information is available at: https://pubs.acs.org/10.1021/acssynbio.1c00537

Author Contributions

K.N. designed the research. C.P.F. and M.H.-T. performed photosynthetic bacterial experiments. K.O. performed the FACS experiment. T.A., H.L., and Y.O. performed the SRS microscopy experiment. C.P.F. and K.N. analyzed the data. The manuscript was written with contributions from all authors. All authors have given approval to the final version of the manuscript.

Notes

The authors declare no competing financial interest.

■ ACKNOWLEDGMENTS

This work was supported by the ImPACT Program of the Council for Science, Technology and Innovation (Cabinet Office, Government of Japan) and JST ERATO (Grant Number JPMJER1602), Japan.

■ REFERENCES

(1) Geyer, R.; Jambeck, J. R.; Law, K. L. Production, Use, and Fate of All Plastics Ever Made. *Sci. Adv.* **2017**, *3*, No. e1700782.
(2) Zheng, J.; Suh, S. Strategies to Reduce the Global Carbon Footprint of Plastics. *Nat. Clim. Change* **2019**, *9*, 374−378.
(3) Trainic, M.; Flores, J. M.; Pinkas, I.; Pedrotti, M. L.; Lombard, F.; Bourdin, G.; Gorsky, G.; Boss, E.; Rudich, Y.; Vardi, A.; Koren, I. Airborne Microplastic Particles Detected in the Remote Marine Atmosphere. *Commun. Earth Environ.* **2020**, *1*, 1−9.
(4) Lomonaco, T.; Manco, E.; Corti, A.; La Nasa, J.; Ghimenti, S.; Biagini, D.; Di Francesco, F.; Modugno, F.; Ceccarini, A.; Fuoco, R.; Castelvetro, V. Release of Harmful Volatile Organic Compounds (VOCs) from Photo-Degraded Plastic Debris: A Neglected Source of Environmental Pollution. *J. Hazard. Mater.* **2020**, *394*, No. 122596.
(5) Bioplastics, E. *Bioplastics Market Data*, 2020.
(6) Meereboer, K. W.; Misra, M.; Mohanty, A. K. Review of Recent Advances in the Biodegradability of Polyhydroxyalkanoate (PHA) Bioplastics and Their Composites. *Green Chem.* **2020**, *22*, 5519−5558.
(7) Suzuki, M.; Tachibana, Y.; Kasuya, K. Biodegradability of Poly(3-Hydroxyalkanoate) and Poly(ε-Caprolactone) via Biological Carbon Cycles in Marine Environments. *Polym. J.* **2021**, *53*, 47−66.
(8) Koller, M. Biodegradable and Biocompatible Polyhydroxy-Alkanoates (PHA): Auspicious Microbial Macromolecules for Pharmaceutical and Therapeutic Applications. *Molecules* **2018**, *23*, 362.
(9) Luo, Z.; Wu, Y. L.; Li, Z.; Loh, X. J. Recent Progress in Polyhydroxyalkanoates-Based Copolymers for Biomedical Applications. *Biotechnol. J.* **2019**, *14*, No. 1900283.
(10) Kourmentza, C.; Plácido, J.; Venetsaneas, N.; Burniol-Figols, A.; Varrone, C.; Gavala, H. N.; Reis, M. A. M. Recent Advances and Challenges towards Sustainable Polyhydroxyalkanoate (PHA) Production. *Bioengineering* **2017**, *4*, 55.

(11) Gomes Gradíssimo, D.; Pereira Xavier, L.; Valadares Santos, A. Cyanobacterial Polyhydroxyalkanoates: A Sustainable Alternative in Circular Economy. *Molecules* **2020**, *25*, 4331.
(12) Higuchi-Takeuchi, M.; Numata, K. Marine Purple Photosynthetic Bacteria as Sustainable Microbial Production Hosts. *Front. Bioeng. Biotechnol.* **2019**, *7*, 258.
(13) Zhang, X.; Lin, Y.; Chen, G.-Q. Halophiles as Chassis for Bioproduction. *Adv. Biosyst.* **2018**, *2*, No. 1800088.
(14) Mitra, R.; Xu, T.; Xiang, H.; Han, J. Current Developments on Polyhydroxyalkanoates Synthesis by Using Halophiles as a Promising Cell Factory. *Microb. Cell Fact.* **2020**, *19*, 86.
(15) Higuchi-Takeuchi, M.; Morisaki, K.; Toyooka, K.; Numata, K. Synthesis of High-Molecular-Weight Polyhydroxyalkanoates by Marine Photosynthetic Purple Bacteria. *PLoS One* **2016**, *11*, No. e0160981.
(16) Foong, C. P.; Higuchi-Takeuchi, M.; Numata, K. Optimal Iron Concentrations for Growth-Associated Polyhydroxyalkanoate Biosynthesis in the Marine Photosynthetic Purple Bacterium *Rhodovulum Sulfidophilum* under Photoheterotrophic Condition. *PLoS One* **2019**, *14*, No. e0212654.
(17) Cai, J.; Wang, G. Hydrogen Production by a Marine Photosynthetic Bacterium, *Rhodovulum Sulfidophilum* P5, Isolated from a Shrimp Pond. *Int. J. Hydrogen Energy* **2012**, *37*, 15070−15080.
(18) Foong, C. P.; Higuchi-Takeuchi, M.; Malay, A. D.; Oktaviani, N. A.; Thagun, C.; Numata, K. A Marine Photosynthetic Microbial Cell Factory as a Platform for Spider Silk Production. *Commun. Biol.* **2020**, *3*, 1−8.
(19) Higuchi-Takeuchi, M.; Motoda, Y.; Kigawa, T.; Numata, K. Class I Polyhydroxyalkanoate Synthase from the Purple Photosynthetic Bacterium *Rhodovulum sulfidophilum* Predominantly Exists as a Functional Dimer in the Absence of a Substrate. *ACS Omega* **2017**, *2*, 5071−5078.
(20) Obruca, S.; Snajdar, O.; Svoboda, Z.; Marova, I. Application of Random Mutagenesis to Enhance the Production of Polyhydroxyalkanoates by *Cupriavidus Necator* H16 on Waste Frying Oil. *World J. Microbiol. Biotechnol.* **2013**, *29*, 2417−2428.
(21) Lee, S. Y.; Kim, H. U. Systems Strategies for Developing Industrial Microbial Strains. *Nat. Biotechnol.* **2015**, *33*, 1061−1072.
(22) Kamravamanesh, D.; Kovacs, T.; Pflügl, S.; Druzhinina, I.; Kroll, P.; Lackner, M.; Herwig, C. Increased Poly-β-Hydroxybutyrate Production from Carbon Dioxide in Randomly Mutated Cells of Cyanobacterial Strain *Synechocystis* Sp. PCC 6714: Mutant Generation and Characterization. *Bioresour. Technol.* **2018**, *266*, 34−44.
(23) Arora, N.; Yen, H.-W.; Philippidis, G. P. Harnessing the Power of Mutagenesis and Adaptive Laboratory Evolution for High Lipid Production by Oleaginous Microalgae and Yeasts. *Sustainability* **2020**, *12*, 5125.
(24) Lee, S.; Kim, P. Current Status and Applications of Adaptive Laboratory Evolution in Industrial Microorganisms. *J. Microbiol. Biotechnol.* **2020**, *30*, 793−803.
(25) Hädicke, O.; Grammel, H.; Klamt, S. Metabolic Network Modeling of Redox Balancing and Biohydrogen Production in Purple Nonsulfur Bacteria. *BMC Syst. Biol.* **2011**, *5*, 150.
(26) Alsiyabi, A.; Immethun, C. M.; Saha, R. Modeling the Interplay between Photosynthesis, CO 2 Fixation, and the Quinone Pool in a Purple Non-Sulfur Bacterium. *Sci. Rep.* **2019**, *9*, 12638.
(27) Kacmar, J.; Carlson, R.; Balogh, S. J.; Srienc, F. Staining and Quantification of Poly-3-Hydroxybutyrate in *Saccharomyces Cerevisiae* and *Cupriavidus Necator* Cell Populations Using Automated Flow Cytometry. *Cytometry A* **2006**, *69A*, 27−35.
(28) Karmann, S.; Follonier, S.; Bassas-Galia, M.; Panke, S.; Zinn, M. Robust At-Line Quantification of Poly(3-Hydroxyalkanoate) Biosynthesis by Flow Cytometry Using a BODIPY 493/503-SYTO 62 Double-Staining. *J. Microbiol. Methods* **2016**, *131*, 166−171.
(29) García-Torreiro, M.; López-Abelairas, M.; Lu-Chau, T. A.; Lema, J. M. Application of Flow Cytometry for Monitoring the Production of Poly(3-Hydroxybutyrate) by *Halomonas Boliviensis*. *Biotechnol. Prog.* **2017**, *33*, 276−284.
(30) Castro, L. M.; Foong, C. P.; Higuchi-Takeuchi, M.; Morisaki, K.; Lopes, E. F.; Numata, K.; Mota, A. J. Microbial Prospection of an Amazonian Blackwater Lake and Whole-Genome Sequencing of Bacteria Capable of Polyhydroxyalkanoate Synthesis. *Polym. J.* **2021**, *53*, 191−202.
(31) Suzuki, Y.; Kobayashi, K.; Wakisaka, Y.; Deng, D.; Tanaka, S.; Huang, C.-J.; Lei, C.; Sun, C.-W.; Liu, H.; Fujiwaki, Y.; Lee, S.; Isozaki, A.; Kasai, Y.; Hayakawa, T.; Sakuma, S.; Arai, F.; Koizumi, K.; Tezuka, H.; Inaba, M.; Hiraki, K.; Ito, T.; Hase, M.; Matsusaka, S.; Shiba, K.; Suga, K.; Nishikawa, M.; Jona, M.; Yatomi, Y.; Yalikun, Y.; Tanaka, Y.; Sugimura, T.; Nitta, N.; Goda, K.; Ozeki, Y. Label-Free Chemical Imaging Flow Cytometry by High-Speed Multicolor Stimulated Raman Scattering. *Proc. Natl. Acad. Sci. U. S. A.* **2019**, *116*, 15842−15848.
(32) Nitta, N.; Iino, T.; Isozaki, A.; Yamagishi, M.; Kitahama, Y.; Sakuma, S.; Suzuki, Y.; Tezuka, H.; Oikawa, M.; Arai, F.; Asai, T.; Deng, D.; Fukuzawa, H.; Hase, M.; Hasunuma, T.; Hayakawa, T.; Hiraki, K.; Hiramatsu, K.; Hoshino, Y.; Inaba, M.; Inoue, Y.; Ito, T.; Kajikawa, M.; Karakawa, H.; Kasai, Y.; Kato, Y.; Kobayashi, H.; Lei, C.; Matsusaka, S.; Mikami, H.; Nakagawa, A.; Numata, K.; Ota, T.; Sekiya, T.; Shiba, K.; Shirasaki, Y.; Suzuki, N.; Tanaka, S.; Ueno, S.; Watarai, H.; Yamano, T.; Yazawa, M.; Yonamine, Y.; Di Carlo, D.; Hosokawa, Y.; Uemura, S.; Sugimura, T.; Ozeki, Y.; Goda, K. Raman Image-Activated Cell Sorting. *Nat. Commun.* **2020**, *11*, 3452.
(33) Coulondre, C.; Miller, J. H. Genetic Studies of the Lac Repressor: IV. Mutagenic Specificity in the *LacI* Gene of *Escherichia Coli*. *J. Mol. Biol.* **1977**, *117*, 577−606.
(34) Foster, P. L. In Vivo Mutagenesis. *Methods Enzymol.* **1991**, *204*, 114−125.
(35) Solovyev, V.; Salamov, A. Automatic Annotation of Microbial Genomes and Metagenomic Sequences. In *Metagenomics and Its Applications in Agriculture, Biomedicine, and Environmental Studies*; Li, R. W., Ed.; Nova Science Publisher's, 2011; pp 61−78.
(36) Tang, K.-H.; Tang, Y. J.; Blankenship, R. E. Carbon Metabolic Pathways in Phototrophic Bacteria and Their Broader Evolutionary Implications. *Front. Microbiol.* **2011**, *2*, 165.
(37) Higuchi-Takeuchi, M.; Numata, K. Acetate-Inducing Metabolic States Enhance Polyhydroxyalkanoate Production in Marine Purple Non-Sulfur Bacteria Under Aerobic Conditions. *Front. Bioeng. Biotechnol.* **2019**, *7*, 118.
(38) Wilkinson, J. H. Enzyme Kinetics and Its Relevance to Enzyme Assay. *J. Clin. Pathol. Suppl.* **1970**, *4*, 14−21.
(39) Cooper, G. M. *The Central Role of Enzymes as Biological Catalysts, Cell: A Molecular Approach*, 2nd edition; Sinauer Associates: Sunderland, MA, https://www.ncbi.nlm.nih.gov/books/NBK9921/ (accessed 2021-12-14).
(40) Takahashi-Íñiguez, T.; Aburto-Rodríguez, N.; Vilchis-González, A. L.; Flores, M. E. Function, Kinetic Properties, Crystallization, and Regulation of Microbial Malate Dehydrogenase. *J. Zhejiang Univ. Sci. B* **2016**, *17*, 247−261.
(41) Carlozzi, P.; Touloupakis, E. Bioplastic Production by Feeding the Marine *Rhodovulum sulfidophilum* DSM-1374 with Four Different Carbon Sources under Batch, Fed-Batch and Semi-Continuous Growth Regimes. *New Biotechnol.* **2021**, *62*, 10−17.
(42) Gordon, G. C.; McKinlay, J. B. Calvin Cycle Mutants of Photoheterotrophic Purple Nonsulfur Bacteria Fail to Grow Due to an Electron Imbalance Rather than Toxic Metabolite Accumulation. *J. Bacteriol.* **2014**, *196*, 1231−1237.
(43) Eprintsev, A. T.; Falaleeva, M. I.; Lyashchenko, M. S.; Toropygin, I. Y.; Igamberdiev, A. U. Oligomeric Forms of Bacterial Malate Dehydrogenase: A Study of the Enzyme from the Phototrophic Non-Sulfur Bacterium *Rhodovulum Steppense* A-20s. *Biosci., Biotechnol., Biochem.* **2018**, *82*, 81−89.
(44) Hansen, T. A.; Veldkamp, H. *Rhodopseudomonas Sulfidophila*, Nov. Spec., a New Species of the Purple Nonsulfur Bacteria. *Arch. Mikrobiol.* **1973**, *92*, 45−58.
(45) Imhoff, J. F. The Alpha-, Beta-, Delta-, and Epsilonproteobacteria. In *Bergey's Manual of Systematic Bacteriology*; Brenner, D. J.,

Krieg, N. R., Staley, J. T., Eds.; Springer, USA: New York, 2005; vol. 2, pp. 205−208.
(46) Maier, R.; Pepper, I. *Bacterial Growth. Environmental Microbiology*, 3rd edition; Elsevier, 2015.
(47) Tillich, U. M.; Lehmann, S.; Schulze, K.; Dühring, U.; Frohme, M. The Optimal Mutagen Dosage to Induce Point-Mutations in *Synechocystis* Sp. PCC6803 and Its Application to Promote Temperature Tolerance. *PLoS One* **2012**, *7*, No. e49467.
(48) Ozeki, Y.; Umemura, W.; Otsuka, Y.; Satoh, S.; Hashimoto, H.; Sumimura, K.; Nishizawa, N.; Fukui, K.; Itoh, K. High-Speed Molecular Spectral Imaging of Tissue with Stimulated Raman Scattering. *Nat. Photon.* **2012**, *6*, 845−851.
(49) Ozeki, Y.; Asai, T.; Shou, J.; Yoshimi, H. Multicolor Stimulated Raman Scattering Microscopy With Fast Wavelength-Tunable Yb Fiber Laser. *IEEE J. Sel. Top. Quantum Electron.* **2019**, *25*, 7100211.
(50) Carver, T.; Thomson, N.; Bleasby, A.; Berriman, M.; Parkhill, J. DNAPlotter: Circular and Linear Interactive Genome Visualization. *Bioinformatics* **2009**, *25*, 119−120.
(51) Kanehisa, M.; Sato, Y.; Kawashima, M.; Furumichi, M.; Tanabe, M. KEGG as a Reference Resource for Gene and Protein Annotation. *Nucleic Acids Res.* **2016**, *44*, D457−D462.
(52) R Core Team. R: A language and environment for statistical computing, http://www.r-project.org/index.html (accessed 2021-07-19).
(53) Wickham, H. *Ggplot2-Elegant Graphics for Data Analysis*; Springer International Publishing: Cham, Switzerland, 2016.
(54) Hothorn, T.; Bretz, F.; Westfall, P. Simultaneous Inference in General Parametric Models. *Biom. J.* **2008**, *50*, 346−363.

https://doi.org/10.1021/acssynbio.1c00537
ACS Synth. Biol. 2022, 11, 909−920